Astron. Astrophys. 315, L353–L356 (1996)

ASTRONOMY
AND
ASTROPHYSICS

Spectrophotometry of UIR bands in the diffuse emission of the galactic disk⋆

K. Mattila[1], D. Lemke[2], L.K. Haikala[1], R.J. Laureijs[3], A. Léger[4], K. Lehtinen[1], Ch. Leinert[2], and P.G. Mezger[5]

[1] Observatory, P.O. Box 14, FIN-00014 University of Helsinki, Finland (mattila at cc.helsinki.fi)
[2] Max-Planck-Institut für Astronomie, Königstuhl 17, D-69117 Heidelberg, Germany
[3] ISO Science Operations Team, ESA - Villafranca, Villafranca del Castillo, Aptdo 50727, E-28080 Madrid, Spain
[4] Institut d'Astrophysique Spatiale, C.N.R.S., Université Paris XI, France
[5] Max-Planck-Institut für Radioastronomie, Postfach 2024, D-53010 Bonn, Germany

Received 16 July 1996 / Accepted 2 August 1996

Abstract. The spectrum of the unidentified infrared (UIR) emission bands between 5.8 and 11.6 μm has been observed for the first time for the *diffuse emission* of the galactic disk where the interstellar radiation field (ISRF) is quite low. The UIR bands at 6.2, 7.7, 8.6, and 11.3 μm have absolute intensities which are $\sim$ 1/10th of the values observed in planetary and reflection nebulae. However, the intensity ratios and band widths are similar, pointing to a common carrier for the UIR bands over a large range of different environmental parameters in the ISM. This mid-IR emission from a low-ISRF medium and the absence of any detectable continuum emission at 10 μm in the diffuse galactic spectra go against any significant contribution from grains at equilibrium temperature or emission during temperature spikes of very small *silicate* grains; it supports the identification of the UIR bands as being due to the PAH molecules.

Key words: interstellar medium: dust – infrared: ISM: bands – Galaxy: general

1. Introduction

The family of the so-called unidentified infrared emission bands (UIR), centered at 3.3, 6.2, 7.7, 8.6, and 11.3 μm, has been observed for more than 20 years (Gillett et al. 1973) in a number of galactic objects, such as planetary nebulae (PN), HII regions, and reflection nebulae (RN) around early type stars, as well as some external galaxies.

There is good evidence for the carriers being some form of carbonaceous material: either large free polycyclic aromatic hydrocarbon molecules (PAHs), or very small grains consisting of hydrogenated amorphous carbon (HACs), quenched carbonaceous composites (QCCs), or coal.

A surprisingly high level of mid-IR emission from the disk of our Galaxy was first detected by Price (1981) and later confirmed by the 12 and 25 μm IRAS observations. Puget et al. (1985) have proposed that this mid-IR emission is largely due to the UIR bands. This proposal has been supported by the photometric detection of the 3.3 μm and 6.2 μm UIR bands in the galactic disk emission (Giard et al. 1988; Ristorcelli et al. 1994). However, no spectra have been obtained for these two bands so far, and for the 7.7, 8.6, and 11.3 μm bands no observations have been reported on the diffuse galactic background emission (hereafter: DGBE).

The present investigation was initiated to answer the following questions: (1) Are the UIR emission bands at 6.2, 7.7, 8.6, and 11.3 μm present also in the diffuse emission of our Galaxy where the UV ISRF is typically 100 – 1000 times lower than in the objects where spectra have been obtained until now? (2) Can the IRAS 12 μm DGBE be explained (solely) as the integrated emission of the UIR bands? (3) What are the relative intensities of the UIR bands in comparison with the bright galactic sources, the PNs, RNs, and the HII regions? (4) What is the spatial distribution of the UIR band carriers in the Galaxy? By finding the answers we hope to contribute also to the problem of identifying the UIR band carriers.

In this letter we present the first results of a guaranteed time project of the ISOPHOT Team. The whole set of observations is intended to include 50 lines of sight, covering the latitudes $b \approx 0°, \pm 1°$, and $\pm 5°$ and the longitudes $l \approx \pm 5°, \pm 15°, \pm 30°, \pm 45°, \pm 60°$. So far the observations cover the longitudes $l = -5°, -30°$, and $-45°$.

⋆ Based on observations made with ISO, an ESA project with instruments funded by ESA member states (especially the PI countries: France, Germany, the Netherlands and the United Kingdom) and with the participation of ISAS and NASA

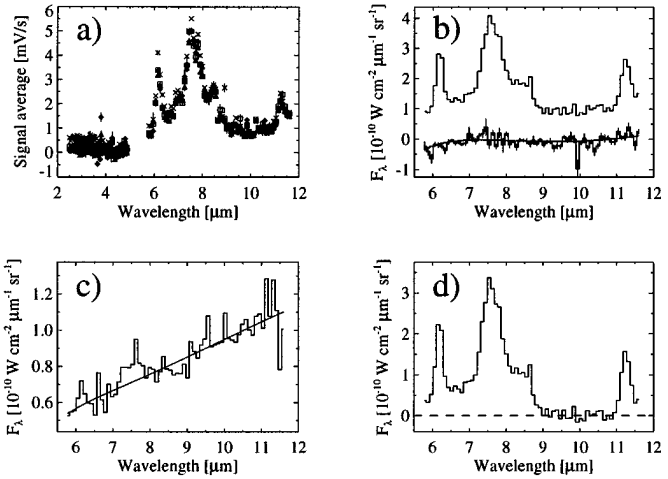

Fig. 1. Illustration of the different reduction steps of the PHT-S spectrum at G-30+0: (a) raw data in instrumental units (mV/sec) for the short (2.5 – 5 μm) and the long-wavelength part (5.8 – 11.6 μm) of the spectrometer; (b) Average 5.8 – 11.6 μm spectrum of 4 raster positions, calibrated and dark current subtracted; dark current with a polynomial fit is shown in the lower part; (c) average of the two OFF-position spectra (at $\pm 5^\circ$) with polynomial fit; (d) final spectrum of the galactic disk emission at G-30+0 with zodiacal light subtracted

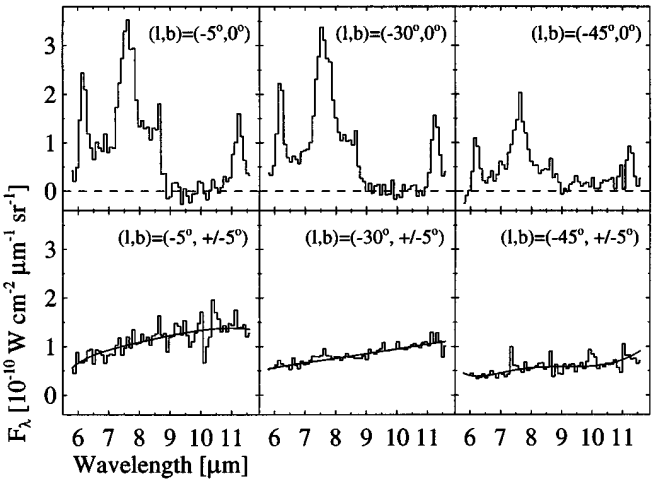

Fig. 2. *Upper panels*: PHT-S spectra of the diffuse galactic emission at b = 0 and $l = -5, -30$, and -45°, as indicated. The zero level is shown as a dashed line. *Lower panels:* The average of the background emission spectra (zodiacal emission) as observed at $b = \pm 5^\circ$

2. Observations and reductions

The positions were selected to avoid any bright IR sources or surface emission, as well as optically bright stars. At each one of the ON positions ($b = 0^\circ, \pm 1^\circ$) we observed with the ISOPHOT low-resolution spectrometer, PHT-S, (cf. Lemke et al. 1996) a 2 × 2 raster and at the OFF positions ($b = \pm 5^\circ$) a 2 × 1 raster map with 64 sec integration time per raster position. The raster step size was 24", i.e. equal to the PHT-S aperture size (24" × 24"). All positions at a given galactic longitude were normally observed in one sequence during the same ISO revolution. This guaranteed that the zodiacal light for the OFF and ON positions referred to the same solar aspect angle.

The data reduction was performed using the Interactive Analysis Program developed by the PHT Consortium.

We illustrate the different reduction steps in Fig. 1 for the position G-30+0. The top panel (a) shows the raw data in instrumental units (mV/s) and with different symbols for the four positions in the 2 × 2 raster map. Both the short- and long-wavelength parts of the spectrometer output are shown in this panel. In the short-wavelength part, in accordance with the expected sensitivity, no signal is seen above the noise level. In the following we do not discuss the short-wavelength PHT-S data any further. The spectra for the four raster positions are seen to agree very well, which confirms that there was no significant contamination by point sources at the selected positions. Panel (b) shows the average of the four positions of the raster map calibrated in physical units (W cm^{-2} μm^{-1} sterad^{-1}). Standard star observations (HR6705 and HR6688) were used for the calibration which is expected to have an absolute accuracy of $\sim$ 20 % in this preliminary phase. The relative intensities within the spectrometer band are estimated to have an uncertainty of $\sim$ 10%. The effect of the uneven beam profile over the 24" × 24" aperture was taken approximatively into account by applying a correction of +25 % to the surface brightnesses. At the bottom of panel (b) the dark current measurement is shown. A polynom has been fitted to the dark current spectrum and has been subtracted from the signal, resulting in the spectrum shown. Clearly, no spectral features (memory effects) above the noise level are present in the dark current spectrum in this case. The subtraction of the zodiacal light is demonstrated by panel (c). The average of the spectra obtained at $b = +5^\circ$ and -5° is shown together with a polynomial fit. No traces of the UIR bands are visible above the noise level. We are therefore confident that this spectrum represents the pure zodiacal light contribution. Only a weak gradient was observed between the $b = \pm 5^\circ$ positions. The zodiacal light level decreases when moving from $l = -5^\circ$ to $l = -45^\circ$, corresponding to ecliptic latitudes from $\beta = -10^\circ$ to $\beta = -42^\circ$ (see Fig. 2). After subtraction of the zodiacal light (fitted line) the final spectrum at G-30+0 for the galactic radiation component is obtained and is shown in panel (d).

3. Results

The resulting PHT-S spectra at $b = 0$ between 5.8 and 11.6 μm are shown in the upper part of Fig. 2. In the lower part we give the average of the zodiacal light spectra as obtained at $b = \pm 5^\circ$. By inspecting these spectra we can immediately list the following results:

(1) The main UIR bands at 6.2, 7.7, 8.6, and 11.3 μm are clearly present in the diffuse galactic emission at $b = 0$ at all longitudes observed and the spectra look similar to those of typical RNs or HII regions. The bands are seen also at the positions $b = \pm 1^\circ$ (except at G-45,-1).

Table 1. The integrated emission of the UIR bands as observed with PHT-S between 5.8-11.6 (= Total) and 7.5-11.6 μm (= LW, long wavelength part) and the IRAS in-band fluxes at 12, 25, 60, and 100 μm. All values are relative to a zero point set at $b = \pm 5^\circ$. Error estimates are given in the last line. The last column gives the ratio of the 5.8 - 11.6 μm integrated UIR intensity to 100 μm IRAS in-band flux

Position		PHT-S		IRAS				
l	b	Tot.	LW	12	25	60	100	$\frac{\text{UIR}}{100}$
		(10^{-10} W cm^{-2} sr^{-1})						
-5.03	0.05	5.1	3.0	5.0	2.0	9.7	16.7	0.31
-30.02	0.17	4.6	2.7	4.4	1.6	7.6	14.6	0.32
-44.60	-0.04	2.5	1.7	2.2	0.8	2.8	5.5	0.45
-29.90	1.00	2.6	1.7	2.9	1.2	4.6	7.0	0.37
		±30%		±15%		±30%		

(2) There is a broad underlying plateau-like emission between 6 and 9 μm. This is in accordance with the findings for e.g. the Orion Bar (Bregman et al. 1989).

(3) The maximum peak emission of the 7.7 μm feature is $\sim$ 3.2 10^{-10} W cm$^{-2}\mu$m^{-1} sterad^{-1}, which is more than a factor 10 fainter than the prototypical RNs or HII regions (e.g. NGC2023, Orion Bar); the difference in the corresponding ISRF intensities is much larger, a factor of $\sim$ 100 to 1000, but the amounts of emitting material are also different.

(4) The level of the "continuum" emission at 9.5 – 10.5 μm is less than 1/10th of the UIR band peaks.

(5) In order to compare the integrated emission of the UIR bands with the IRAS 12 μm emission we have summed up the PHT-S spectra between 7.5 and 11.6 μm (the IRAS band pass covers $\sim$ 7.5 μm to 15 μm). The results are shown in Table 1. It can be seen that, at the very least, $\sim$ 50 – 60 % of IRAS 12 μm emission is due to the UIR bands. If the UIR bands of the DGBE are similar to the highly illuminated regions also in the 11.6 to 15 μm range it is possible that the *whole* IRAS 12μm emission can be explained in terms of the UIR bands.

The average ratio of the integrated UIR band intensity (5.8 - 11.6 μm) to the IRAS in-band intensities at 12, 25, 60, and 100 μm is 1.0, 2.7, 0.65, and 0.36, respectively. Using the average spectral energy distribution of the galactic IR emission as given in Désert et al. (1990, their Fig. 4) we can estimate that the total IR flux of the large grains is $\sim$ 2.5 times the IRAS 60+100 μm flux. Thus, using the data in Table 1 we can estimate that the energy absorbed by the UIR carriers is $\sim$ 10 % relative to the large grains.

(6) The UIR band wavelengths and widths. We have fitted the spectra with four Cauchy line profiles. The central wavelengths and linewidths (FWHM) are as follows: 6.19 μm (0.20 μm), 7.64 μm (0.71 μm), 8.51 μm(0.42 μm), and 11.26 μm (0.27 μm). These values agree well with the wavelengths and widths observed for the RNs and HII regions.

4. Discussion and conclusions

We have observed for the first time the spectra of the UIR bands between 5.8 and 11.6 μm in the diffuse emission of the galactic disk. The detection level achieved with the PHT-S spectrometer in $\sim$ 4 min integration time is by a a factor of $\sim$ 10 lower than what has so far been possible with ground-based (in limited wavelength bands) or air-borne telescopes.

1. General properties. Despite the much lower level of emission, per unit mass, and the different environment of interstellar space which is probed by our DGBE spectra, the basic properties and ratios of the UIR bands are surprisingly similar to the objects with a much higher radiation field, the PNs, RNs, and HII regions. This demonstrates that the carriers of the UIR bands are very resistant to different interstellar environmental and ageing effects. Also, if the UIR bands are caused by a mixture of different molecule/grain populations their relative abundances and physical parameters (e.g. ionization) must be remarkably constant or, alternatively, the spectral characteristics of the different molecules/grains must be very similar. In order to produce thermal emission at the level observed in the UIR peaks of our DGBE spectra one needs a temperature of $\geq$ 100 K. Such high *equilibrium* temperatures cannot be reached by grains in the very low ISRF of the diffuse ISM. Thus our observation of mid-IR emission in the UIR bands *excludes an equilibrium emission* and points to emission during thermal spikes.

2. The 10μ*m continuum.* We address first the question whether the weakness of the observed continuum at 10 μm could be due to the broad silicate absorption feature centered at 9.7 μm. This absorption has been observed in the diffuse medium towards local as well as galactic center background sources. In the galactic center region, with a strong continuum *background* level, the *foreground* silicate absorption could account for a more than 90 % reduction of the 10 μm continuum. In our case where we have a mixture of emitting and absorbing particles, distributed over a long column, the reduction factor is much smaller, however. We have estimated that the silicate absorption does not suppress the 10 μm diffuse galactic continuum by more than 30 - 50 % in the observed longitude range. We can thus place a silicate-absorption-corrected upper limit of $F_\lambda \leq 0.4$ 10^{-10} W cm^{-2} μm^{-1} sterad^{-1}to the 10 μm continuum.

A clear difference between our DGBE and the PN and RN spectra is seen in the 10 μm continuum level. This continuum is ascribed to very small grains or PAH clusters which in the PNs and RNs are transiently heated to sufficiently high temperatures to emit at 10 μm. In the case of the diffuse ISM (our spectra) we do not detect any noticeable 10 μm continuum. Especially, the contribution during temperature spikes by very small *silicate* grains, which would emit strongly in the band centered at 9.7 μm, must be very small (see discussion by Désert et al. 1986). We consider this as a strong argument in favor of the PAH model for the UIR bands.

3. Galactic distribution. Using the 7.7 μm line height we have estimated that for an exponential latitude distribution the FWHM is $1.3 \pm 0.2^\circ$. ¿From IRAS 12 μm data at the same positions we find a value of $1.5 \pm 0.1^\circ$. In the longitude direction the band intensities at $l = -5^\circ$ and -30° are almost equal while at $l = -45^\circ$ the intensity is about half of it. This again agrees with the IRAS 12μm distribution. The ratio of the integrated UIR band intensity (5.8-11.6 μm) to IRAS 100 μm flux (see Table 1) has at $l = -45^\circ$ ($b = 0$) a value of 0.45 which is, given

Table 2. Line ratios of the UIR bands in different objects: in the galactic disk (DGBE) according to the present study, in planetary nebulae (PN), reflection nebulae (RN), and HII regions (HII) according to Cohen et al. 1989

	$\frac{I_\lambda(6.2)}{I_\lambda(7.7)}$	σ	$\frac{I_\lambda(11.3)}{I_\lambda(7.7)}$	σ
DGBE	**0.23**		**0.24**	
	(0.19 - 0.30)		(0.16 - 0.30)	
PN	0.41	$\pm$ 0.06	0.29	$\pm$0.07
RN	0.68	$\pm$ 0.07	0.22	$\pm$0.05
HII	0.58	$\pm$ 0.04	0.29	$\pm$0.04

the statistical uncertainties of the data of $\sim \pm 10\%$, larger than the values at $l = -5$ and $-30°$. A comparison with the analysis of the IRAS 12/100 μm ratio by Giard et al. (1994) suggests that most of this difference is due to extinction in the 6-12 μm band and does not imply a changing UIR carrier-to-dust ratio.

4. Line ratios. The line intensities (line areas) I_λ were determined from the Cauchy fits as heigth $\times$ FWHM. The height of the 6.2 μm band was counted from the plateau emission "continuum" interpolated between 5.8 and 6.5 μm. For the 7.7 μm band, the average value between 6.6 and 7.0 μm was adopted as "continuum" level. Thus our 6.2 and 7.7 μm line intensities refer solely to the well-defined sharper spectral structures, in accordance with the procedure adopted by Cohen et al. (1989).

The line ratios $I_\lambda(6.2\mu m)/I_\lambda(7.7\mu m)$ and $I_\lambda(11.3\mu m)/I_\lambda(7.7\mu m)$ as observed for DGBE are given in Table 2 together with a compilation of Cohen et al. (1989) for PNs, RNs and HII regions. Average values calculated from the four positions (-5,0), (30,0), (-45,0), and (-30,1) are given in the first line. The range of values is given in the second line in parentheses, and it indicates the statistical and point-to-point scatter of the DGBE values. Furthermore, a systematic uncertainty due to calibration of $\sim$ 10 % should be added.

In the PAH model the 6.2 and 7.7 μm bands are due to the C – C stretching vibrations. Thus one can assume, in the first approximation, that this ratio is relatively insensitive to composition changes in the PAHs. Different processes, such as ionization, or differences in the molecular size distribution could change the line ratio $I_\lambda(6.2\mu m)/I_\lambda(7.7\mu m)$. Another possible explanation for the smaller value of the ratio in the DGBE is that it is a temperature effect (cf. Léger et al. 1989): a lower line ratio in the DGBE would indicate a lower PAH fluctuation temperature, which is in accordance with the lower energy of individual UV ISRF photons in the diffuse medium compared with the PNs, RNs, and HII regions.

In the PAH model the 11.3 μm band is due to the C – H out-of-plane bending vibrations. The lower ionization degree of the PAHs away from strong UV fields would predict that the line ratio $I_\lambda(11.3\mu m)/I_\lambda(7.7\mu m)$ is *larger* in the diffuse ISM as compared to the PNs, RNs and HII regions (for a discussion of the effects of ionization cf. Allamandola et al. 1995). Furthermore, one would expect that the higher hydrogenation and lower temperature of the PAHs in the diffuse ISM influence the ratio in the same direction. Thus, it is surprising that the observed line ratio $I_\lambda(11.3\mu m)/I_\lambda(7.7\mu m)$ in the DGBE is so similar to the values in the higher radiation field sources.

Acknowledgements. We gratefully acknowledge the funding of the ISOPHOT experiment by the Deutsche Agentur für Raumfahrtangelegenheiten (DARA) and financial support for this research project by the University of Helsinki Research Fund, the Academy of Finland, and the Max-Planck Society. We are grateful to Dr. U. Herbstmeier for help during the data analysis and to an anonymous referee for useful comments.

References

Allamandola, L.J., Sandford, S.A., Hudgins, D.M., Witteborn, F.C., 1995, PASP Conf. Ser. 73, 23
Bregman, J., Allamandola, L.J., Tielens, A.G.G..M., Geballe, T.R., Witteborn, F.C., et al.,1989, ApJ 344,791
Cohen, M., Tielens, A.G.G.M., Bregman, J.D. et al. 1989, ApJ 341,246
Désert, F.X., Boulanger, F., Léger, A., Puget, J.L., Sellgren, K., et al.,1986, A&A 159, 328
Désert, F., Boulanger, F., Puget, J., 1990, A&A 237, 215
Giard, M., Pajot, F., Lamarre, J.M. et al., 1988, A&A 201, L1
Giard, M., Lamarre, J.M., Pajot, F., Serra, G., 1994, A&A 286, 203
Gillett, F.C., Forrest, W.J., Merrill, K.M., 1973, ApJ 183, 87
Léger, d'Hendecourt, L., Défourneau, D., 1989, A&A 216, 148
Lemke, D. et al., 1996, A&A , this issue
Price,S., 1981, AJ 86, 193
Puget, J.L., Léger, A., Boulanger, F., 1985, A&A 142, L19
Ristorcelli, I., Giard, M., Meny, C. et al., 1994, A&A 286, L23